Research in Astronomy and Astrophysics, 25:035016 (12pp), 2025 March

https://doi.org/10.1088/1674-4527/adbb56
CSTR: 32081.14.RAA.adbb56

Research on Rationally Oversampled Channelization Algorithm for Ultra-wideband Signals

Xu Du[1,2], Hai-Long Zhang[1,2,3,4], Shao-Cong Guo[5], Ya-Zhou Zhang[1], Jie Wang[1,4], Xin-Chen Ye[1,4], Jian Li[1,2], Wen-Na Cai[1,2], Han Wu[1,2], and Ting Zhang[1,2]
[1] Xinjiang Astronomical Observatory, Chinese Academy of Sciences, Urumqi 830011, China; zhanghailong@xao.ac.cn
[2] University of Chinese Academy of Sciences, Beijing 100049, China
[3] Key Laboratory of Radio Astronomy, Chinese Academy of Sciences, Nanjing 210008, China
[4] National Astronomical Data Center, Beijing 100101, China
[5] Southeast University, Nanjing 211189, China
Received 2024 December 3; revised 2025 February 18; accepted 2025 February 24; published 2025 March 18

Abstract

To address the issues of low accuracy and high computational complexity in traditional channelization techniques for ultra-wideband signals, this paper proposes a novel rationally oversampled channelization method to enhance the accuracy and efficiency of signal processing. The proposed method is evaluated by implementing and comparing critically sampled and integer oversampled channelization algorithms. A detailed analysis of the impact of different oversampling factors and filter orders on performance is provided. The validity of the proposed algorithm is verified using baseband data from pulsar J0437−4715 observed by the Parkes telescope, demonstrating its effectiveness and correctness.

Key words: (stars:) pulsars: general – methods: data analysis – techniques: miscellaneous

1. Introduction

With the continuous advancement of modern technology, astronomical observation techniques are rapidly evolving, placing increasing demands on signal processing methods. In the context of astronomical observations, signal processing and transmission are critical, as they directly affect the accuracy and reliability of the observed data. Ultra-WideBand (UWB) signals, characterized by their exceptionally broad frequency ranges, are typically defined as signals with a relative bandwidth exceeding 0.25 or an absolute bandwidth greater than 500 MHz (Sabath et al. 2005). These signals exhibit broad spectral coverage in the frequency domain and extremely short pulses in the time domain, posing significant challenges for their processing (Wu & Wnag 2024).

Channelization technology, which decomposes wideband or ultra-wideband signals into multiple narrowband, plays a crucial role in improving the flexibility and efficiency of signal processing (Tang et al. 2018). Astrophysical phenomena such as pulsars and Fast Radio Bursts (FRBs) exhibit pronounced transient characteristics (Zhang et al. 2024) and extremely broad spectral bandwidth (e.g., FRBs exhibit spectral coverage extending to several GHz). The full-bandwidth output data rate of Qi-Tai Telescope (QTT) UWB receive system reaches 208 Gb s^{-1}. The channelization of astronomical UWB signals is a necessary step, but traditional methods often struggle to balance accuracy, efficiency, and flexibility, limiting their applicability in demanding scenarios. In critically sampled channelizer, insufficient subband edge attenuation leads to fan-shaped loss. In the integer oversampling channel, under the limitation of fixed oversampling factors (e.g., 2×, 3×), it shows low bandwidth utilization (50% effective data rate), which puts significant pressure on the storage system and transmission system of long-term observation projects such as pulsar time array.

To address these limitations, this study proposes a novel rationally oversampled channelization method for UWB signals in radio astronomy. While critically sampled channelization algorithms are efficient and avoid redundant data generation, they are limited by aliasing and lack flexibility (Morrison et al. 2020). In contrast, integer oversampled channelization algorithms offer higher accuracy and better data recovery but require increased bandwidth. The rationally oversampled channelization algorithm provides a balanced solution, offering improved accuracy, reduced data bandwidth, and greater flexibility, making it particularly suitable for processing UWB signals in dynamic astronomical environments.

Tuohutinuer et al. implemented a polyphase filter bank based on CUDA, effectively improving the processing power and computational efficiency of radio astronomical observation data by leveraging the floating-point computation and efficient parallel execution capabilities of graphics processors (Tohtonur & Zhang 2017). This approach is essentially based on a critically sampled channelization algorithm. George Hobbs et al. used the Xilinx Kintex FPGA development board to

divide the 3328 MHz bandwidth data captured by the UWB receiver into 26 sub-bands, each 128 MHz wide, using a critically sampled polyphase filter bank. The data was then transmitted to the Medusa gpu processing unit for further processing. They plan to use oversampling techniques for channelization in the future to prevent signal attenuation at the edges of sub-bands and effectively mitigate aliasing effects (Hobbs et al. 2020).

The QTT will use a UWB receiver to observe astronomical signals in the 150 MHz–115 GHz frequency range (Wang et al. 2023). Its UWB low-frequency receiver, with a bandwidth of 704–4032 MHz, will be deployed first. For the QTT's UWB signal, Zhang Hailong et al. designed a signal division scheme and verified the critically sampled channelization algorithm using simulated UWB pulsar baseband data (Zhang et al. 2023). Zhang Meng et al. applied a 2× oversampled polyphase filter bank to divide the J0437−4715 observation data into 16 sub-bands, and after removing redundant data, recombined the sub-bands into a wideband signal. The resulting signal closely resembled the original observation data, yielding a more ideal pulse profile than the critically sampled polyphase filter bank (Zhang et al. 2023).

Jia Bocheng et al. applied a 2× oversampled channelizer at the Onsala space observatory to achieve real-time capture of FRBs (Jia & Chen 2021). Smith et al. implemented a 4 GHz, 4096-branch, 8-tap, 2× oversampled channelizer on an RFSoC using HLS, applying it to frequency-division multiplexing microwave resonator detectors without requiring hardware description languages. They plan to expand the design in the future to accommodate arbitrary fractional decimation rates (Smith et al. 2021).

In this study, the rationally oversampled channelization algorithm is implemented using Python and applied to process real astronomical data. The results after channelization are displayed and compared with the original data. Additionally, the pulsar profile is plotted to verify the correctness of the channelization algorithm. By comparing the performance of the critically sampled channelization, integer oversampled channelization, and rationally oversampled channelization algorithms, the potential advantages of the proposed method are highlighted.

2. Rationally Oversampled Channelization Algorithm

The structure diagram of the rationally oversampled channelization algorithm proposed in this paper is shown in Figure 1. In this diagram, $x[0]$, $x[1]$, … represent the input data, the red section indicates the commutator, and M denotes the number of channels. z^{-1} represents the delay unit. The commutator is a key component of the channelization algorithm. Its main function is to distribute the input signal across multiple filters. Specifically, the commutator alternately assigns the sample points of the input signal to different filters in a certain order, enabling the polyphase processing of the signal (Harris et al. 2024). The design of the commutator must ensure that the signal sequence received by each filter correctly represents a sub-band of the original signal.

The filter is the core part of the channelization algorithm. Each filter is responsible for processing a specific sub-band of the input signal. When designing the filter, several factors need to be considered, including filter order, window function selection, and hardware resources. The filter order determines both the complexity and performance of the filter. A higher filter order improves the frequency response accuracy but increases computational complexity and hardware resource consumption. The choice of window function also affects the filter's passband and stopband characteristics. In this paper, the Hamming window is used, as it strikes a good balance between main lobe width and side lobe attenuation. The moderate main lobe width provides better frequency resolution, while the faster side lobe attenuation helps reduce side lobe leakage (Price 2021).

This algorithm modifies the filter structure of the integer oversampled channelization algorithm, as shown in Figure 2. Here $h_n[t]$ represents the tth filter coefficient of the nth filter. $\otimes$ indicates the multiplier, and $\oplus$ represents the adder. Similar to integer oversampled, zero padding is required between adjacent filter coefficients. However, since it is not possible to insert a fractional number of zeros, the zero padding operation must be performed in two steps. First, the coefficients are reshaped into M rows, where M is the number of channels in the filter bank, and each row corresponds to the filter coefficients of a particular filter. Then, $T =$ Numerator of reduced fraction$(\frac{M}{D}) - 1$ zeros are inserted between adjacent coefficients of the original filter, thereby increasing the sampling rate to an integer multiple of the original rate. The original filters are then split into $X =$ Denominator of reduced fraction$(\frac{M}{D})$ individual sub-filters.

In rationally oversampled channelization algorithms, the initial decimation's system function is expressed as:

$$H(z) = \sum_{n=-\infty}^{\infty} h(n) z^{-n} \tag{1}$$

This represents the convolution of the input signal with the system's impulse response $h(n)$ in the frequency domain. Through polyphase decomposition, it can be reformulated as:

$$\begin{aligned} H(z) &= \sum_{i=0}^{M-1} \left[\sum_{m=-\infty}^{\infty} h(mM - i) z^{-mM} \right] z^{i} \\ &= \sum_{i=0}^{M-1} H_i(z^M) z^i \end{aligned} \tag{2}$$

In this decomposition, the filter's impulse response $h(n)$ is partitioned into M subsequences, each corresponding to a specific phase. Here, i denotes the phase index, ranging from 0 to $M - 1$, and m represents the time index of the decimated

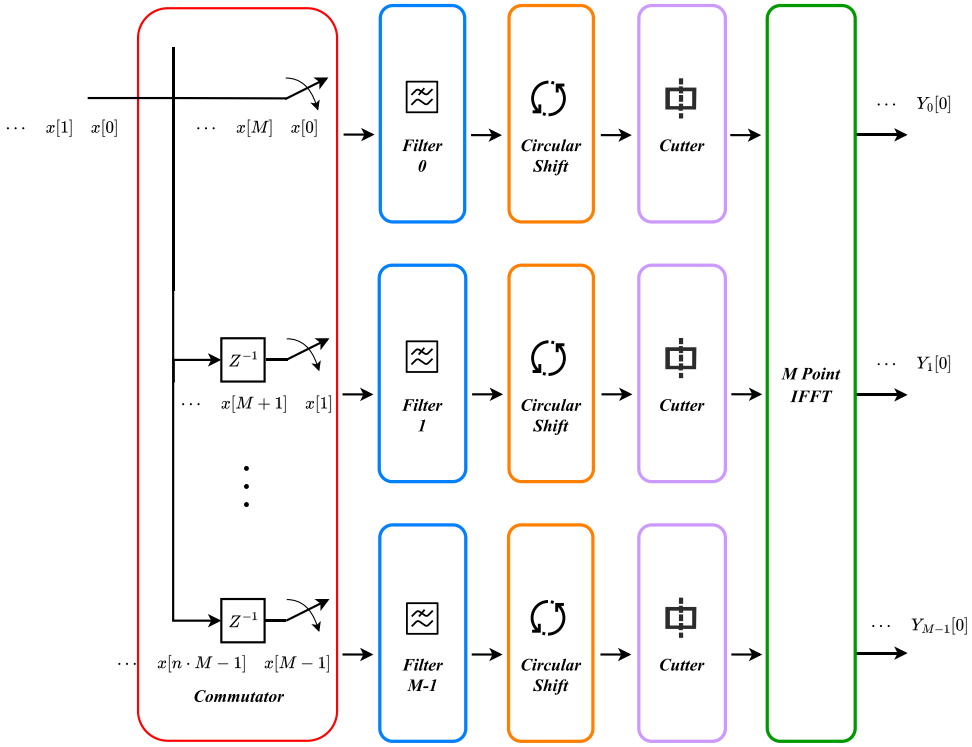

Figure 1. Structure diagram of the rationally oversampled channelization algorithm.

sequence for each sub-filter. Each subsequence corresponds to a sub-filter $H_i(z)$, defined as:

$$H_i(z) = \sum_{m=-\infty}^{\infty} h(mM - i)z^{-m} \tag{3}$$

This indicates that the system function of each sub-filter $H_i(z)$ is the z-transform of the impulse response sequence corresponding to that phase. The m is the time index of the subfilter, indicating the position of the filter coefficient within each multiphase branch. For the ith multiphase branch, the subfilter coefficient is extracted from the original filter $h(n)$ by interval M. Through this decomposition, the original filter $H(z)$ can be represented as a combination of these sub-filters, where each sub-filter processes a decimated data of the original input. The z-transform of the output signal can be expressed as:

$$\begin{aligned} Y_k(z) &= \frac{1}{D}\sum_{i}^{D-1} U_k(z^{\frac{1}{D}}W_D^i)H_i(z^{\frac{M}{D}}W_D^{iM}) \\ W_D^k &= e^{-j\frac{2k\pi}{M}} \end{aligned} \tag{4}$$

Here U_k represents the delay of the kth polyphase branch. This design allows flexible configuration of the oversampling factor and data bandwidth in the channelization algorithm. We use $M = 8$ and $D = 6$ as an example, and the transformation diagram of the rationally oversampled coefficients is shown in Figure 3(a).

In the rationally oversampled channelization algorithm, the data to be filtered must be repeated. First, the one-dimensional input data is reshaped into M rows. Then, an overlap operation is performed on the reshaped data. Given that the number of channels $M = 8$ and the decimation factor $D = 6$, the proportion of repeated data is $1/4$, meaning that the data $x[6]$ and $x[7]$ from $x[0]\ldots x[7]$ are repeated, as shown in the "Overlap Data" in Figure 3(b). Additionally, an offset operation is performed, where the number of "Offset Data" equals the number of sub-filters, namely X. The offset for each "Offset Data" is $gcd(M, D)$. The offset data is then split and reorganized into new sub-filter data, and the corresponding sub-filter coefficients are convolved and summed, yielding the result of the $8/6\times$ rationally oversampled channelization. The transformation diagram of rationally oversampled data is shown in Figure 3(b).

The orange portion in Figure 1 is often called a circular shifter or circular buffer. The circular shifter ensures that the data maintains the correct phase relationship throughout the processing. Since the non-maximum decimation channelization algorithm induces phase rotation in each output sub-band, the circular shifter adjusts the data position to correct the phase rotation caused by oversampling, thus maintaining the accuracy of the results. The step size for each shift is defined as

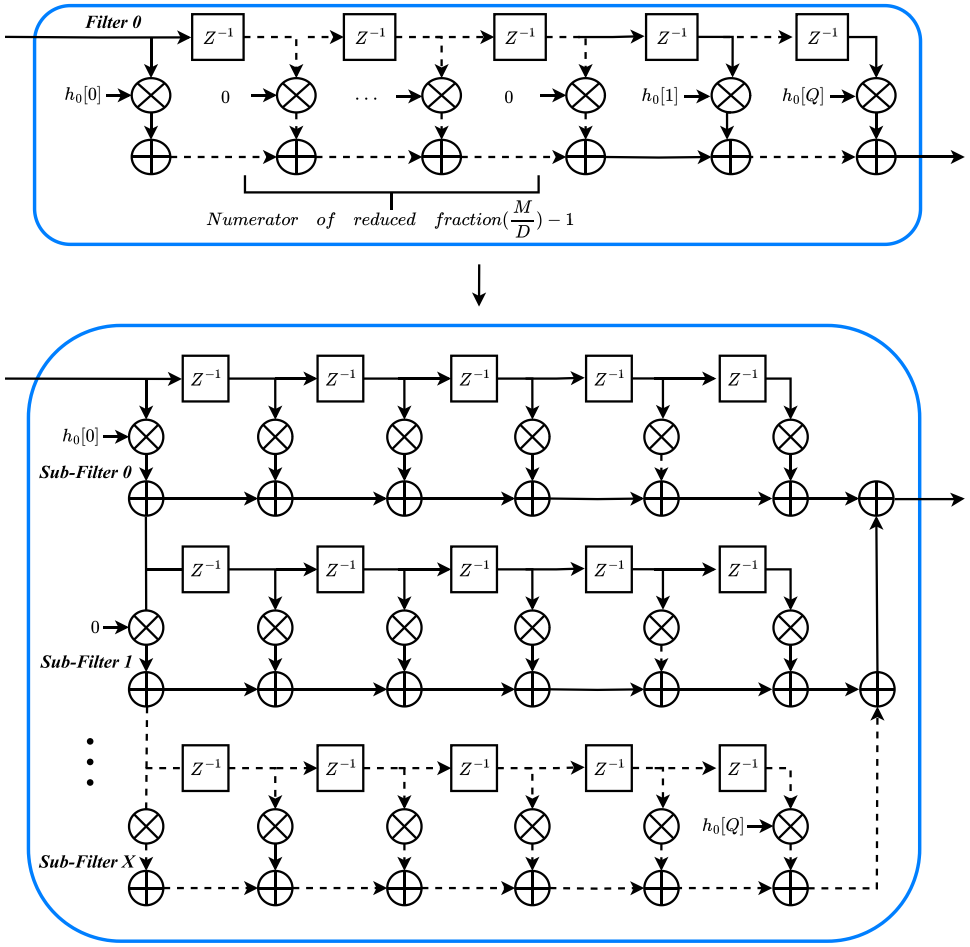

Figure 2. Structure diagram of rationally oversampled channelization algorithm.

$MoveStep = (MoveStep + M - D) \bmod M$, where the initial value of $MoveStep$ is 0. The main difference between the integer oversampled channelization algorithm and the proposed method lies in the step size, which varies from the total number of states. For instance, with parameters such as $M = 20$, $D = 15$, and $Oversample\ Factor = \frac{20}{15} = \frac{4}{3}$, the detailed circular shift steps are given. The step sizes for each circular shift are 0, 5, 10, 15, and each round of the circular shift has $\frac{M}{M-D} = 4$ states, as shown in States 0 to 3 in Figure 4. State 4 represents the first state of the next round of circular shifts. The data after circular shift is then processed by a cutter, followed by IFFT or FFT.

The cutter eliminates redundant data within each sub-band signal. In the oversampled channelization algorithm, the bandwidth of each sub-band is M/D times that of the critically sampled channelization algorithm. In the integer oversampled channelization algorithm, the sub-band bandwidth is at least twice that of the critically sampled algorithm, resulting in redundant data between adjacent sub-bands. The cutter removes this redundancy, retaining only D/M of the data. Different approaches to the cutter have been presented in literature (Zhang et al. 2023). In this paper, the cutter retains $[0] \sim [D/M * \text{Size}]$ data as the result of each channel, where $\text{Size} = \text{length}(\text{FFT}(Y))$, and Y represents the output after IFFT. The channelization algorithm implemented in this paper is open-sourced.[6]

The green section in Figure 1 is the M-point IFFT, which can also be implemented using FFT. The primary difference between the two is that the input data order is reversed in FFT (Renfors et al. 2017), but in this paper, the IFFT is used. $Y_n[t]$ represents the tth data output by the nth channel of the IFFT.

3. Experimental Analysis and Results

In this study, the algorithm was implemented in Python and used to process tagged signal data and complete astronomical

[6] https://github.com/WhataDavid/Channelizer

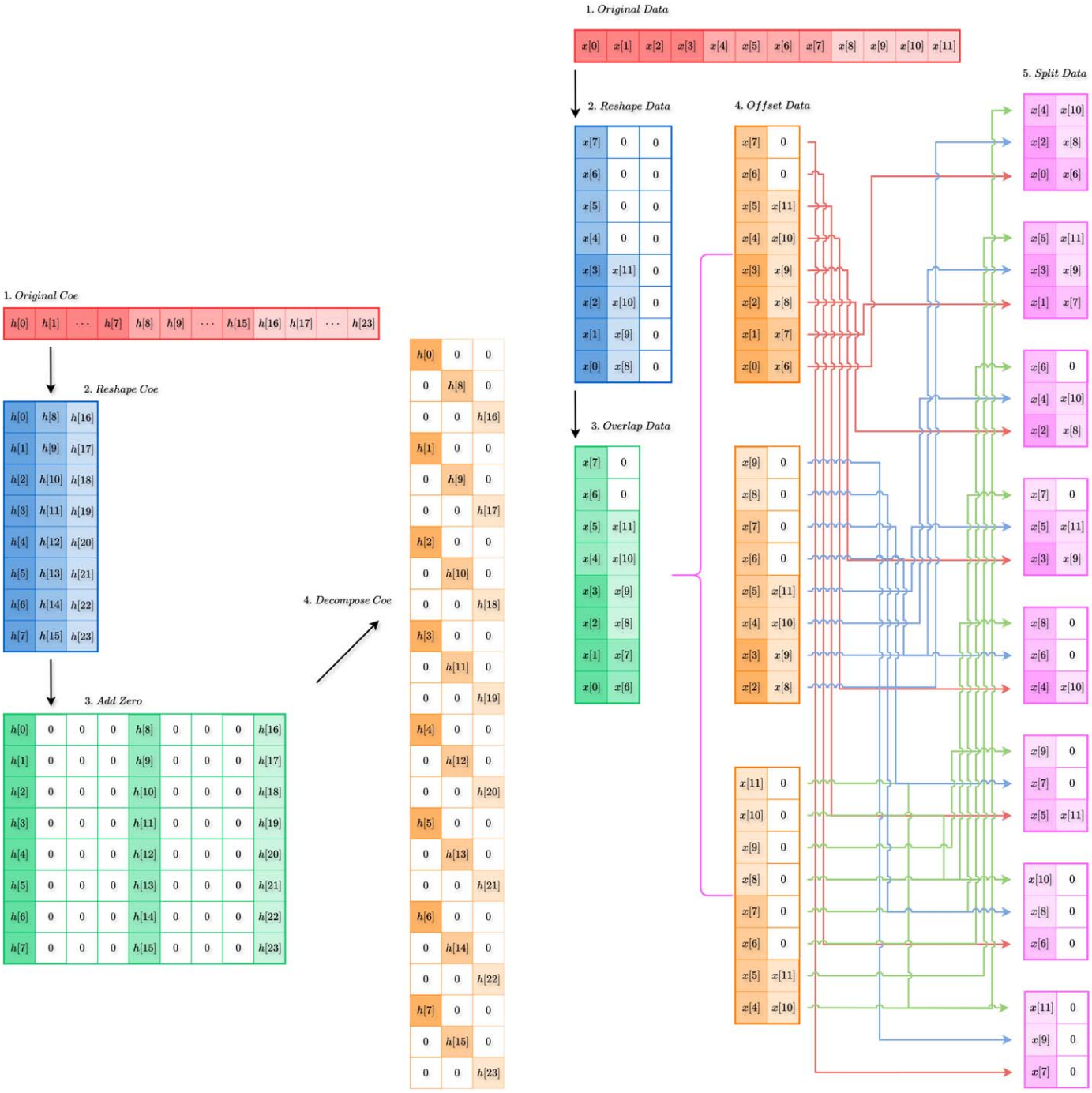

(a) Transformation diagram of the rationally oversampled coefficients

(b) Transformation diagram of rationally oversampled data

Figure 3. Transformation diagrams of rationally oversampled coefficients and data.

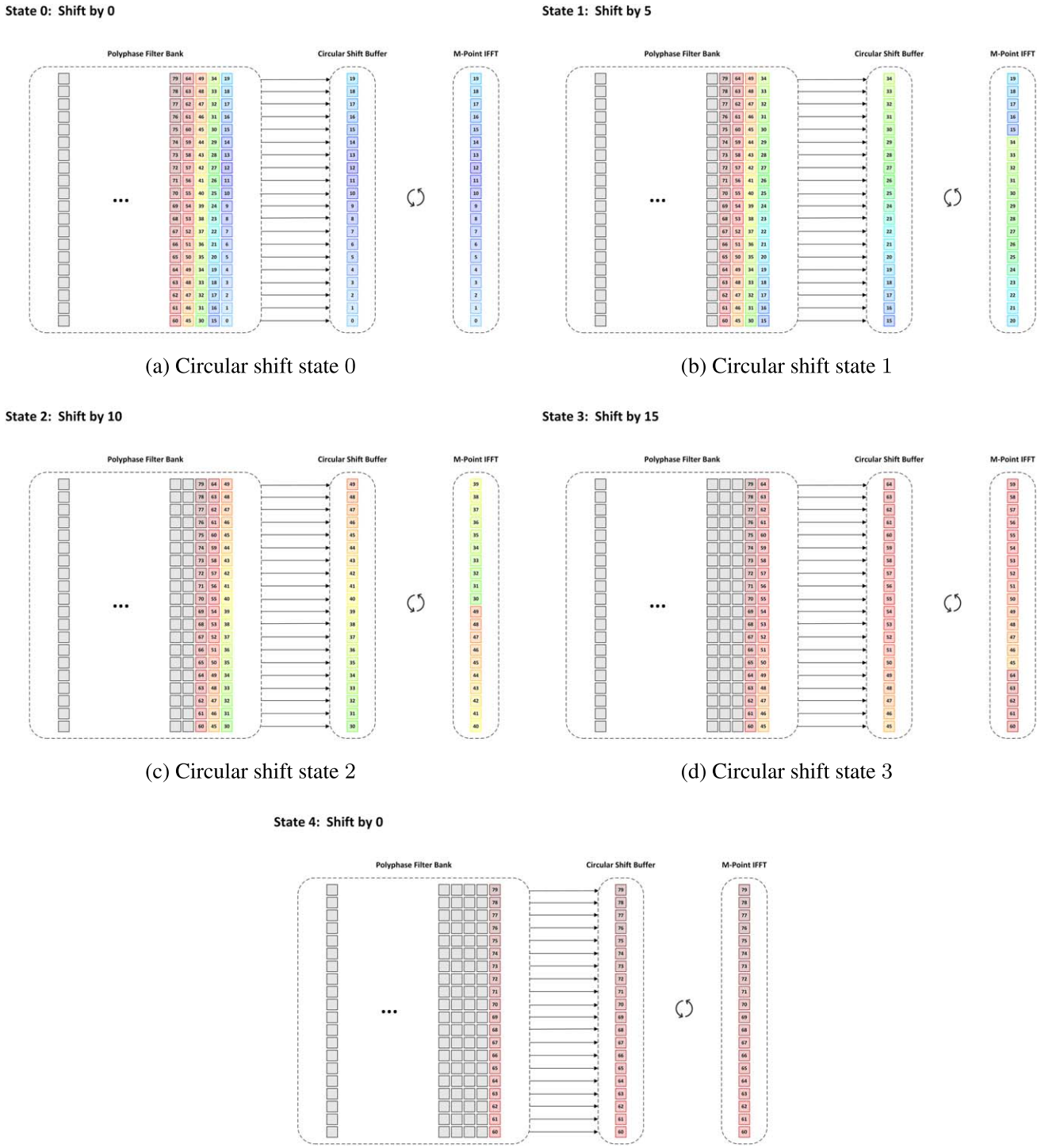

(a) Circular shift state 0

(b) Circular shift state 1

(c) Circular shift state 2

(d) Circular shift state 3

(e) Circular shift state 0 of the next round

Figure 4. Details of the circular shift state diagrams.

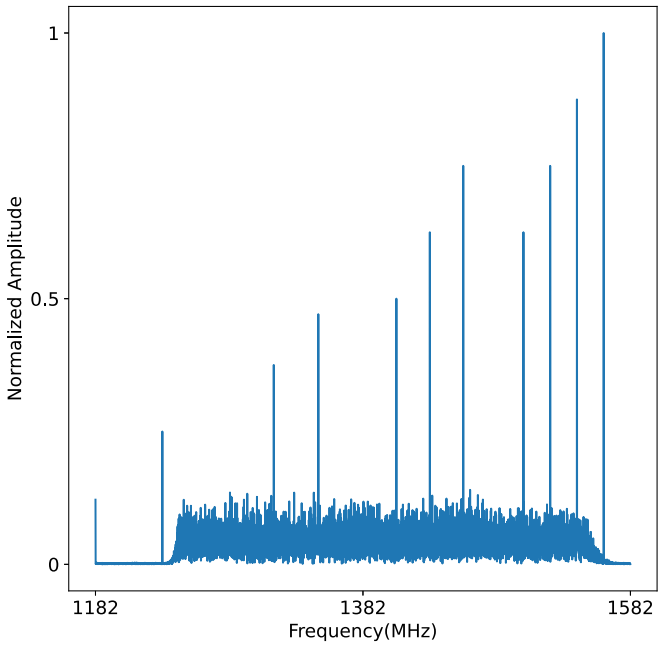

Figure 5. Spectrum of test data containing tagged signals.

Table 1
Observation Data Information of J0437−4715

Parameters	J0437–4715
Cfreq (MHz)	1382
Bandwidth	400
Nbit	8
Npol	2
Folding period (s)	0.00575730363767324
DM (cm^{-3} pc)	2.64476
Tsamp (ms)	0.00125
Observation time (s)	8
File size (GB)	11.9

data to validate its correctness. The original data consists of pulsar data from J0437−4715, with an observation duration of 8 s, a bandwidth of 400 MHz, a center frequency of 1382 MHz, and a dispersion measure (DM) of 2.64476 cm^{-3} pc, as detailed in Table 1.

3.1. Processing of Data with Tagged Signals

First, 12,800 data points are extracted for the channelization experiment to quickly validate the correctness of the rationally oversampled channelization algorithm. Some tagged signals are added to the extracted data, we added multiple tagged signals to each channel with the same number as the channel serial number and increasing signal amplitude to distinguish mirror signals. The spectrum of the test data containing tagged signals is shown in Figure 5.

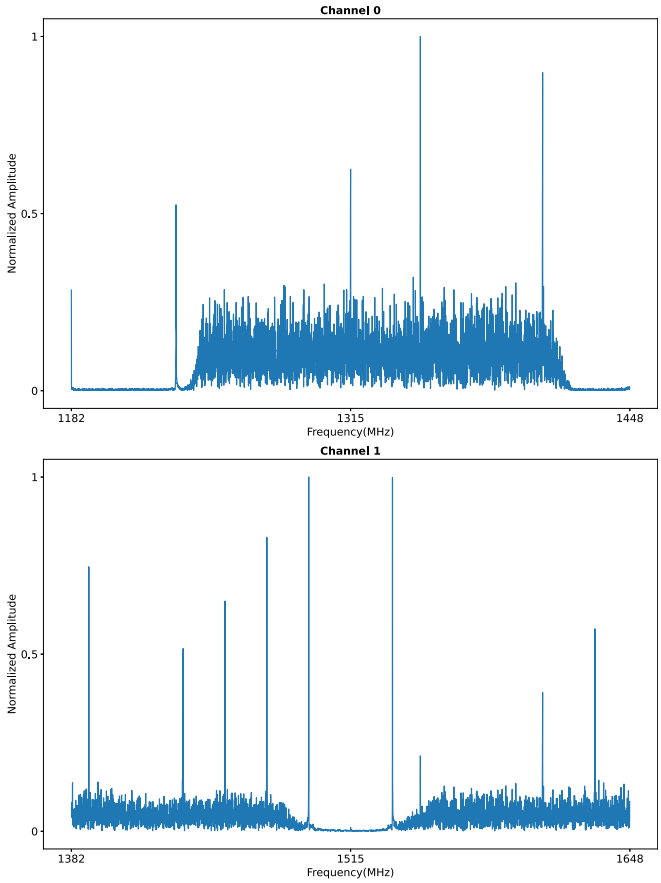

Figure 6. Spectrum after polyphase filtering.

The test data is channelized using the rationally oversampled channelization algorithm with $M = 4$ and $D = 3$. The spectrum after polyphase filtering is shown in Figure 6. Due to the conjugate symmetry of the obtained data, only the results for one half of the channels are presented.

As shown in Figure 6, the tagged signals have been split, but the result appears disordered, which is caused by phase interlacing due to oversampling. After applying the circular shifter, the spectrum of each channel is shown in Figure 7.

The result after processing with the circular shifter clearly shows that the phase of the tagged signal has been corrected; however, redundant data remains. Due to oversampling, the bandwidth of the sub-band signal is increased, introducing data from other channels. The cutter is then applied to remove the redundant data. The result after cutting is shown in Figure 8. The test data containing the tagged signal has been successfully channelized.

3.2. Processing of Data with Complete Signals

Subsequently, the complete 8 s J0437−4715 observation data was experimentally verified. Since the total size of the data

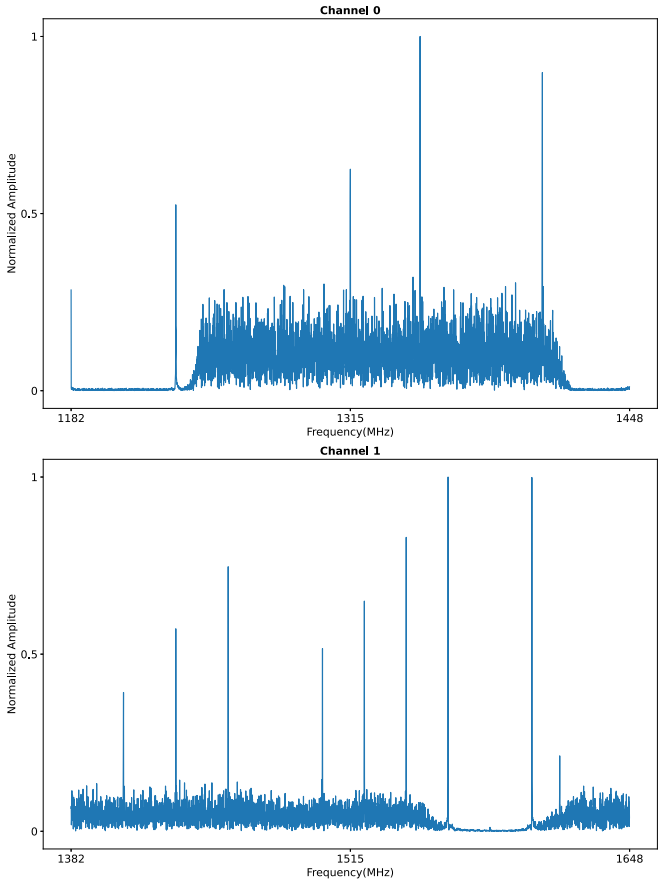

Figure 7. Spectrum after circular shifter.

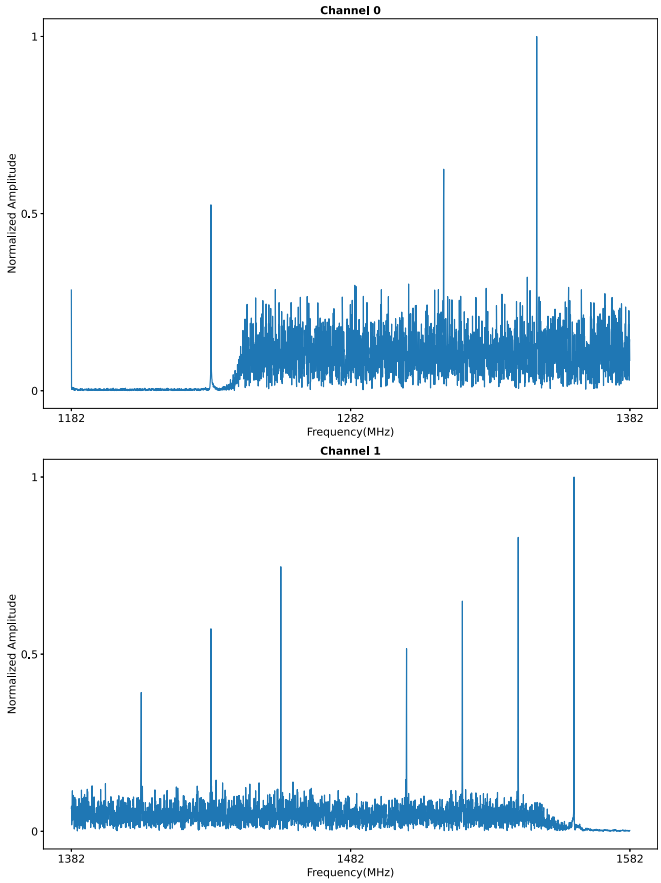

Figure 8. Spectrum after cutter.

is 11.9 GB, it was processed in 190 blocks. Each block is 2^{25} bytes in size, and the spectrum of the first block of data is shown. The figure includes the spectra of polarization 1 and polarization 2, with the orange spectrum representing polarization 1 and the blue spectrum representing polarization 2. The spectrum of the first block of the original data is shown in Figure 9(a). After applying the critically sampled channelization algorithm, the integer oversampled channelization algorithm, and the rationally oversampled channelization algorithm, the spectra of the first block of data after channellization algorithm are shown in Figures 9(b), (c) and (d), respectively. From the figures, it can be seen that when a 32-order FIR filter based on the Hamming window is used in each channel, the critically sampled channelization algorithm exhibits a distinct fan-shaped loss at the channel edges, resulting in significant data distortion. In contrast, the spectra from the integer oversampled and rationally oversampled channelization algorithms are closer to the original data, indicating better recovery of the original signal.

When the filter order is reduced, the disadvantages of the critically sampled channelization algorithm become more pronounced. The fan-shaped loss is amplified, while the integer oversampled and rationally oversampled channelization algorithms provide better data results than the critically sampled channelization algorithm, even at lower FIR filter orders. The results are shown in Figures 10(a) through (d).

After processing all the block data with the rationally oversampled channelization algorithm, a dispersion delay diagram for each channel is generated, as shown in Figure 11. Each sub-band correctly displays the pulse profile. Since the number of divided channels is $M = 20$ and the data is complex, only half of the data, i.e., 10 channels, is shown for clarity. Among these, the first channel contains minimal pulse information, making it impossible to integrate a pulse profile similar to those of the other channels. As the number of channels decreases, a more coherent pulse profile can be obtained. Figure 12 presents the phase spectrum diagram of the sub-band without alignment, where the green strip represents the pulse information. Figure 13 shows the phase spectrum diagram of the sub-band after coherent dispersion elimination and alignment, where the pulse is accurately aligned. Finally, Figure 14 displays the pulse profile after channelization and dispersion correction using the rationally oversampled

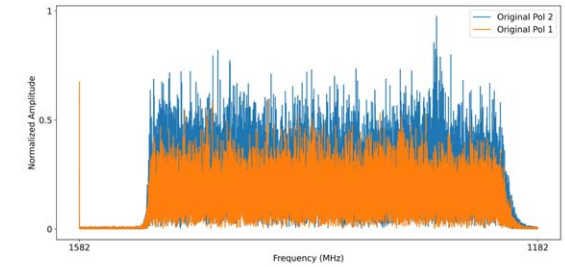

(a) Original data

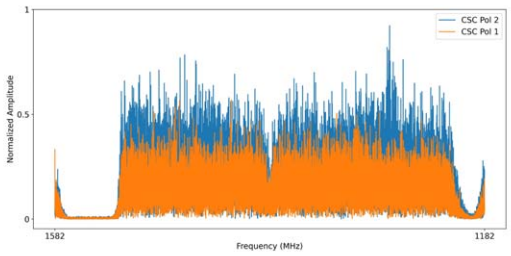

(b) 32-order critically sampled channelizer

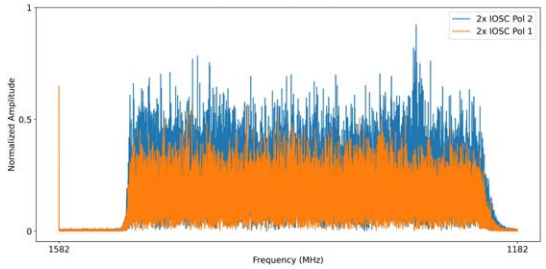

(c) 32-order $2\times$ integer oversampled channelizer

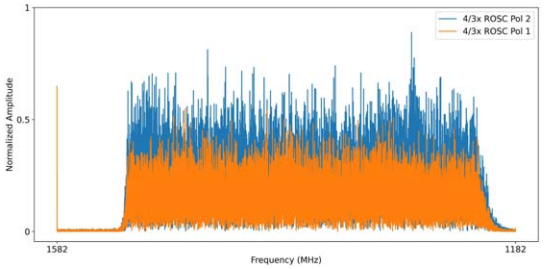

(d) 32-order $4/3\times$ rationally oversampled channelizer

Figure 9. Effect of oversampling factor on channelization.

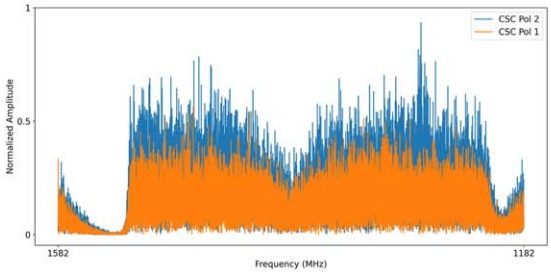

(a) 8-order critically sampled channelizer

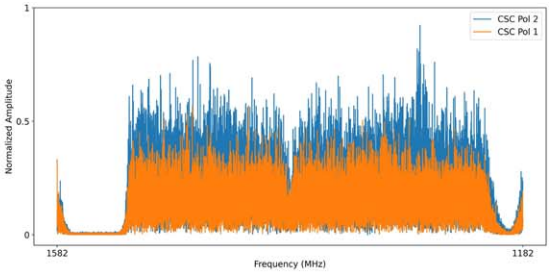

(b) 32-order critically sampled channelizer

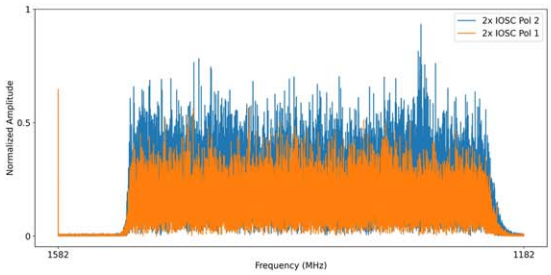

(c) 8-order $2\times$ integer oversampled channelizer

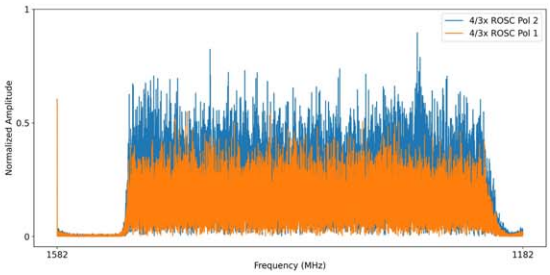

(d) 8-order $4/3\times$ rationally oversampled channelizer

Figure 10. Effect of filter order on channelization.

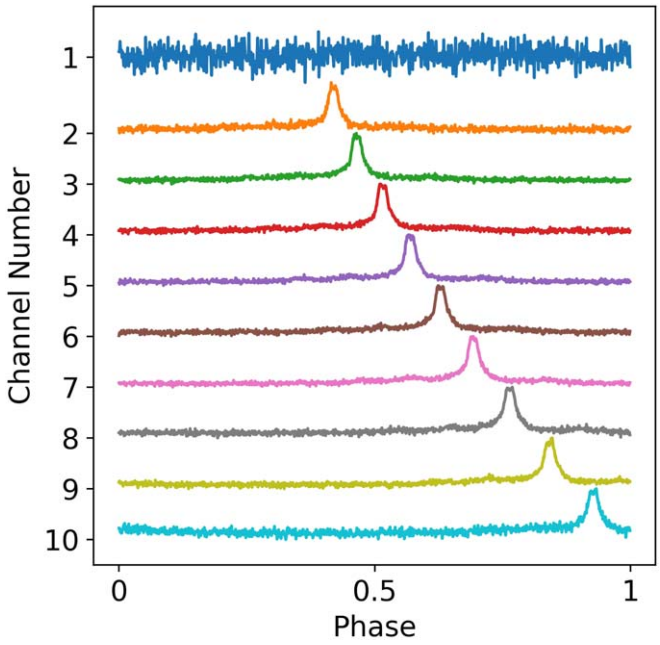

Figure 11. Sub-band dispersion delay diagram of the rationally oversampled channelization.

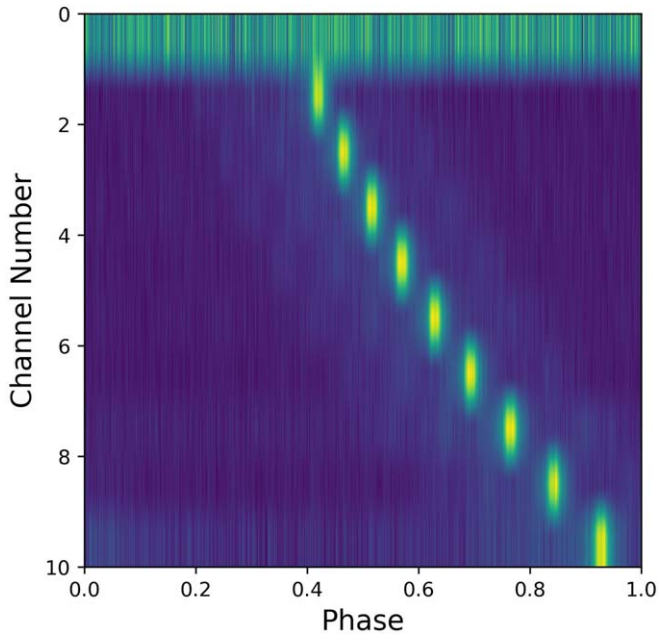

Figure 12. Sub-band phase frequency spectrum of rationally oversampled channelization (not aligned).

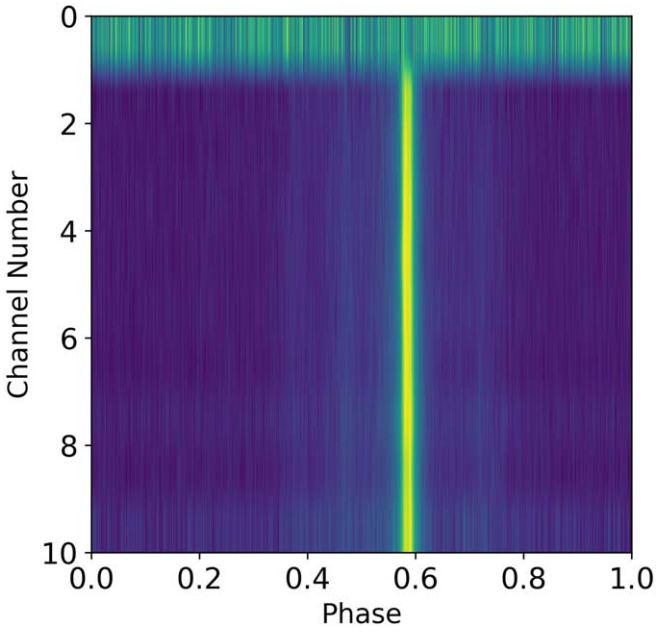

Figure 13. Sub-band phase diagram of rationally oversampled channelization algorithm (aligned).

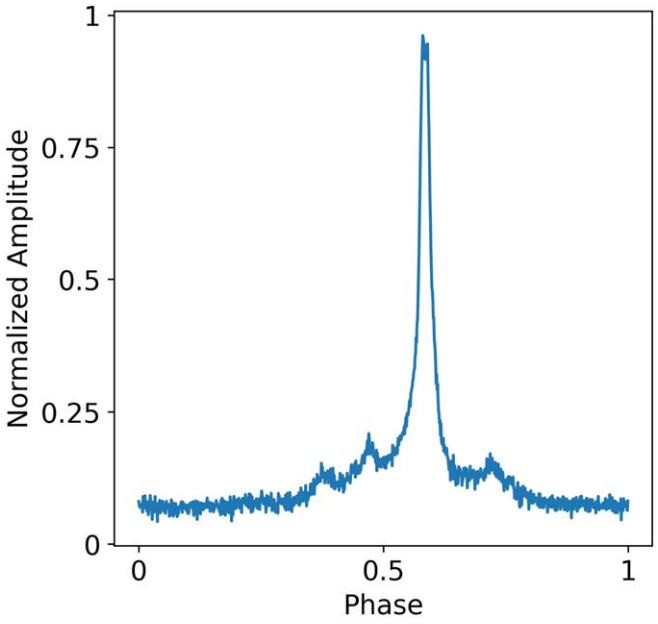

Figure 14. Pulse profile spectrum of rationally oversampled channelization algorithm.

channelization algorithm. The pulse profile in the figure confirms the correctness of the algorithm.

The execution time of the channelization algorithm with different oversampling factors is compared. Using an Intel i9-9900K@3.60 GHz processor and 64 GB of RAM, the time taken for channelization of 11.9 GB of UWB data is shown in Table 2. The execution efficiency of the critically sampled channelization algorithm is the highest, with its processing time being less than half that of the oversampled channelization

Table 2
Comparison of Execution Time for Different Channelization Algorithms

Type	Execution Time (s)
Critical sampling channelization	9282
Integer oversampled channelization	22105
Rationally oversampled channelization	22742

Table 3
Comparison of Applicable Situation for Different Channelization Algorithms

Type	Applicable Situation
Critical sampling channelization	Tense computing resources, low transmission rate, small storage space, long observation time, and low accuracy requirements
Integer oversampled channelization	Abundant computational resources, high transmission rate, large storage space, short observation time, and high accuracy requirements
Rationally oversampled channelization	Abundant computational resources, low transmission rate, medium storage space, short observation time, and high accuracy requirements

algorithms. This is because it eliminates the cycle shift and cut operation. The execution time of the integer oversampled channelization algorithm is comparable to that of the rationally oversampled channelization algorithm.

By comparing three different channelization algorithms with varying oversampling factors, it is found that the sub-bands of these algorithms exhibit different accuracy and data bandwidth, which directly influence subsequent data processing. Additionally, the observation time and requirements vary for each observer. The applicability of each channelization algorithm is summarized in Table 3.

4. Conclusion

Aiming to address the challenges of low accuracy in the critically sampled channelization algorithm and the large bandwidth in the integer oversampled channelization algorithm for UWB signal processing, a rationally oversampled channelization algorithm is designed and implemented. This algorithm is based on the concept of rational oversampling factors. The algorithm was experimentally validated using the baseband data of pulsar J0437−4715, observed with the Parkes telescope. By comparing the performance of the critically sampled channelization algorithm, the integer oversampled channelization algorithm, and the rationally oversampled channelization algorithm, it is found that the rationally oversampled approach offers significant advantages in balancing accuracy and data bandwidth. The experimental results demonstrate that the rationally oversampled channelization algorithm effectively divides the UWB signal and yields the correct pulse profile. Future plans include deploying the algorithm on FPGA and finding ways to reduce the computational load, such as developing a lightweight filter architecture based on CORDIC to replace the traditional multiply accumulate unit and reduce the utilization of logic resources. Aimed at molecular spectral line observation data, we adjust the algorithm to adapt to it.

Acknowledgments

This work is supported by the National Key R&D Program of China Nos. 2021YFC2203502 and 2022YFF0711502; the National Natural Science Foundation of China (NSFC) (12173077); the Chinese Academy of Sciences (CAS) “Light of West China” Program (No. xbzg-zdsys-202410); the Tianshan Talent Project of Xinjiang Uygur Autonomous Region (2022TSYCCX0095 and 2023TSYCCX0112); the Scientific Instrument Developing Project of the Chinese Academy of Sciences, grant No.PTYQ2022YZZD01; China National Astronomical Data Center (NADC); the Operation, Maintenance and Upgrading Fund for Astronomical Telescopes and Facility Instruments, budgeted from the Ministry of Finance of China (MOF) and administrated by the Chinese Academy of Sciences (CAS); Natural Science Foundation of Xinjiang Uygur Autonomous Region (2022D01A360).

ORCID iDs

Xu Du https://orcid.org/0000-0001-6448-0822
Hai-Long Zhang https://orcid.org/0000-0002-8951-7094
Ya-Zhou Zhang https://orcid.org/0000-0001-6046-2950
Jie Wang https://orcid.org/0000-0003-0380-6395

References

Harris, F., Morgenstern, H., & Ohayon, E. 2024, in 2024 IEEE 67th Int. Midwest Symp. Circuits and Systems (MWSCAS) (Piscataway, NJ: IEEE), 211

Hobbs, G., Manchester, R. N., Dunning, A., et al. 2020, PASA, 37, e012

Jia, B., & Chen, X. 2021, A Fast Radio Burst (FRB) Capture System for the Onsala Space Observatory, Master's thesis, Chalmers Univ. Technology

Morrison, I., Bunton, J., van Straten, W., Deller, A., & Jameson, A. 2020, JAI, 9, 2050004

Price, D. C. 2021, The WSPC Handbook of Astronomical Instrumentation: Volume 1: Radio Astronomical Instrumentation (Singapore: World Scientific), 159

Renfors, M., Mestre, X., Kofidis, E., & Bader, F. 2017, Orthogonal Waveforms and Filter Banks for Future Communication Systems (New York: Academic)

Sabath, F., Mokole, E. L., & Samaddar, S. 2005, URSB, 2005, 12

Smith, J. P., Bailey, J., Tuthill, J., et al. 2021, IEEE Open Journal of Circuits and Systems, 2, 241

Tang, Z., Zhu, D., & Pan, S. 2018, JLwT, 36, 4219

Tohtonur, H., & Zhang, J. W. 2017, A Design of Polyphase Filter Bank for Radio Astronomy Based on CUDA, AR&T, 14, 117

Wang, N., Xu, Q., Ma, J., et al. 2023, SCPMA, 66, 289512

Wu, S.-f., & Wnag, F. 2024, A study of the assessment metric based on catalogs for radio interferometric imaging, Journal of Guangzhou University (Natural Science Edition), 23, 58

Zhang, H., Wang, J., Zhang, Y., et al. 2024, AstTI, 1, 1

Zhang, H.-L., Zhang, Y.-Z., Zhang, M., et al. 2023, RAA, 23, 125023

Zhang, M., Zhang, H.-L., Zhang, Y.-Z., et al. 2023, RAA, 23, 085012